Bidirectional CO_2 Desorption in Steady-State CO Oxidation on Rh(110)

Izabela I. Rzeźnicka[†] and Tatsuo Matsushima*[,†,‡]

Graduate School of Environmental Earth Science, Hokkaido University, Sapporo 060-0810, Japan, and Laboratory of Surface Reaction Dynamics, Catalysis Research Center, Hokkaido University, Sapporo 060-0811, Japan

Received: December 11, 2002; In Final Form: May 1, 2003

The angular and velocity distributions of desorbing product CO_2 were studied in steady-state CO oxidation on Rh(110) by means of cross-correlation time-of-flight techniques and low-energy electron diffraction. In the limited CO pressure range in the active region, where the reaction was fairly first order in CO, the angular distribution in the plane including the [001] direction abruptly changed from a normally directed form into bidirectional lobes collimated at ±24° from the surface normal. At the same time, the CO_2 productivity was enhanced, and the (1 × 2) LEED pattern due to the missing-row structure was observed. The translational temperature of desorbing CO_2 was maximized at these collimation angles. The metastable (1 × 2) missing-row structure was proposed to be responsible for this CO_2 formation. However, in the inhibited region, where CO retarded the reaction, desorbing CO_2 was thermalized to the surface temperature.

I. Introduction

Desorbing product CO_2 from CO oxidation on noble metal surfaces carries a high excess of translational energy.[1,2] The repulsive force exerted by its formation site on the product is strong enough to hold the site orientation and symmetry in the angular and velocity distributions. The product-formation site can be identified from these distributions, as demonstrated by angle-resolved thermal desorption spectroscopy (AR-TDS).[3] A (110) plane of noble metals is reconstructed into missing-row forms when it is clean or covered by O(a).[4] In fact, reactive CO_2 desorption is bidirectionally split along the local normal of declining terraces on reconstructed Pt(110) and Ir(110), indicating CO_2 formation on inclined (111) facets of the missing-row structure.[5,6] However, no bidirectional desorption has been found on Pd(110)[7] and Rh(110),[8] although these are reconstructed by oxygen adsorption. This paper delivers the first observation of bidirectional CO_2 desorption on Rh(110). It was observed at limited reactant pressures under steady-state CO oxidation conditions.

The Rh(110) surface easily undergoes reconstruction by oxygen adsorption and forms different superstructures depending on the coverage and the surface temperature.[9−11] The well-ordered missing-row structure seems to be formed only around an oxygen coverage of $\Theta_O = 0.5-0.35$ and after annealing above 700 K. The bidirectional CO_2 desorption may be scarcely observed by AR-TDS because this method must scan over a wide range of reactant coverage and surface temperature.[12] However, steady-state CO oxidation may yield suitable conditions to keep the missing-row structure in the active region, where oxygen coverage gradually changes with CO pressure. In steady-state CO oxidation on platinum metal, there is a critical CO pressure at which the rate-determining step switches from CO adsorption to O_2 dissociation.[13,14] Below the critical pressure (the active region), the amount of O(a) is generally higher than that of CO(a) and decreases toward zero with increasing CO pressure. The metastable (1 × 2) missing-row form prepared by removing O(a) by CO or hydrogen is rather stable up to 480 K.[15,16] There must be suitable conditions for the active missing-row structure, although surface species may not sharply switch over close to the critical point when separate domains are formed.[17] The velocity measurements under such limited conditions can be performed by means of steady-state angle-resolved measurements[18] and not by modulated molecular beam scatterings because the chopping of incoming beams causes the oxygen and CO coverages to change throughout the conditions critical for chemical kinetics.[2]

II. Experiment

The apparatus consists of a reaction chamber, a chopper house, and an analyzer.[19] All of the chambers are evacuated by individual pumping systems. The reaction chamber has LEED and XPS optics, an Ar^+ gun, and a quadrupole mass spectrometer (QMS). In the second chamber, the chopper disk with a pseudo-random slit sequence[20] is rotated at 98.04 Hz, yielding a time resolution of 20 μs. The arrival times at the ionizer of another QMS in the analyzer were registered on a multichannel scalar running synchronously with the chopper rotation. A Rh(110) single crystal of 10-mm diameter and 1-mm thickness was mounted on top of a manipulator. The crystal was rotated to change the desorption angle (θ, polar angle) in a plane including the [001] direction.[21,22] The partial pressures of ^{13}CO (P_{CO}) and O_2 (P_{O2}) were kept constant by dosing gases continuously. Hereafter, the isotope ^{13}C is simply designated as C.

During AR steady-state measurements, the chopper disk was stopped at the position where an open slot was in front of the slit between the reaction chamber and the chopper house. The steady-state CO_2 formation rate was monitored in both angle-integrated (AI) and angle-resolved (AR) forms. The rate in the former was determined by QMS in the reaction chamber as the difference in the CO_2 signal between the desired surface temperature (T_S) and room temperature. In the latter, it was obtained by QMS in the analyzer chamber as the difference

* Corresponding author. E-mail: tatmatsu@cat.hokudai.ac.jp.
† Graduate School of Environmental Earth Science.
‡ Catalysis Research Center.

10.1021/jp022574r CCC: $25.00
Published on Web 07/22/2003

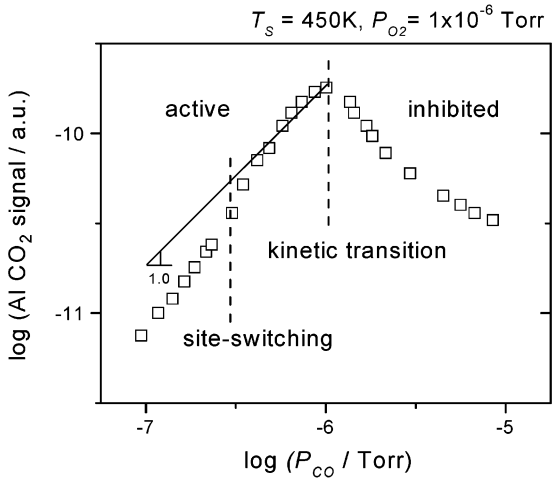

Figure 1. Variation of the steady-state CO_2 desorption rate observed in the AI form as a function of CO pressure at $P_{O_2} = 1.0 \times 10^{-6}$ Torr and $T_S = 450$ K. The vertical broken lines show the site-switching and kinetic transition points.

(ΔCO_2) between the signal at the desired angle and the signal when the crystal was away from the line-of-sight position. The sharpness of the angular distribution is underestimated when the AR signal is plotted without corrections due to QMS sensitivity differences between molecules with different velocity, but the collimation angle is not shifted because the velocity is maximized at this angle.[23]

III. Results

A. General Features. The steady-state CO_2 formation rate became observable above $T_S = 400$ K, was maximized at around 480 K, and then decreased with a further increase of T_S. The dependence on the CO pressure was characterized by a sharp transition to higher productivity in the middle of the active region and a fast decrease above the kinetic transition, as shown in the AI form in Figure 1.

This enhancement was remarkable at around $\theta = 24°$, as confirmed in AR measurements. The signals observed at $\theta = 0$ and 24° are shown in Figure 2a. Both signals showed a common critical CO pressure where the reaction changed from near first order to negative orders in CO. The former region is called the "active region," and the latter, the "inhibited region." It should be noticed that the signal at $\theta = 24°$ runs below that at $\theta = 0°$ at lower CO pressures and around the middle of the active region overcomes the other (i.e., the angular distribution sharply changes from the normally directed to a bidirectional form). The former is named "active A," and the latter,"active B." A slow distribution change begins in active A because the signal enhancement at $\theta = 24°$ is slightly faster than that at $\theta = 0°$, as shown by different slopes. The preference of the signal at the normal direction is recovered at higher CO pressures, even below the kinetic transition. Above the transition pressure, the signal in the normal direction is always higher than that at $\theta = 24°$.

B. Angular Distribution. Sharp changes were found in the angular distribution of desorbing CO_2 at the boundary between active A and B. This boundary, at which the CO_2 signal at $\theta = 24°$ becomes equal to that at $\theta = 0°$, is called "site switching" because of the sharp angular distribution change.[24] At CO pressures below this point (active A), the CO_2 desorption was collimated along the surface normal, whereas it was split into the bidirectional form above this point. This splitting became unclear with increasing CO pressure below the kinetic transition.

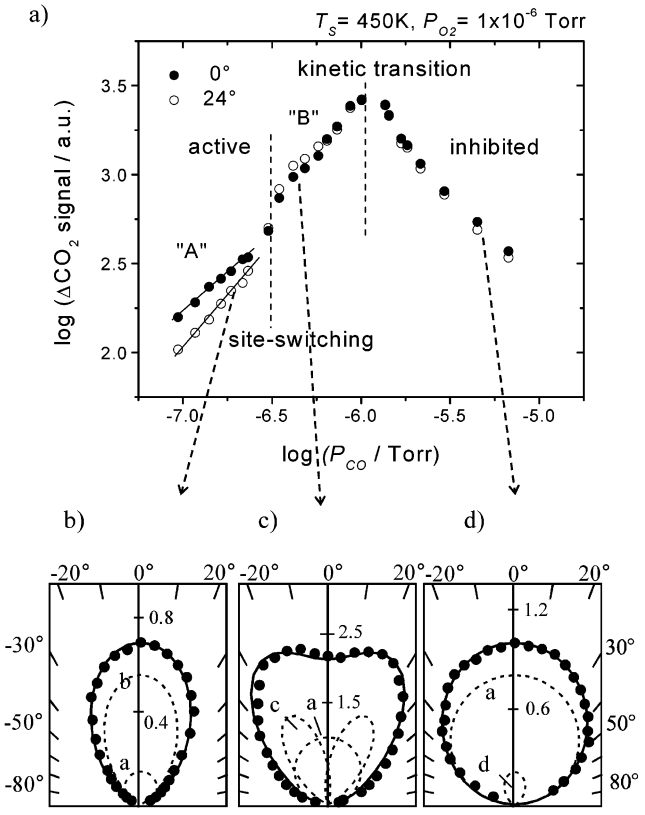

Figure 2. (a) Variation of the steady-state CO_2 desorption rate observed at $\theta = 0°$ (●) and 24° (○) as a function of CO pressure at $T_S = 450$ K and $P_{O_2} = 1.0 \times 10^{-6}$ Torr. (b−d) Angular distributions of CO_2 in the plane along the [001] direction and typical deconvolutions are shown in polar coordinates. The ordinate was normalized to the signal in the normal direction in the inset (c). P_{CO} is (b) 2.2×10^{-7} Torr, (c) 4.2×10^{-7} Torr and (d) 4.5×10^{-6} Torr. The components drawn by broken curves show a, $\cos(\theta)$; b, $\cos^4(\theta)$; c, $\cos^{10}(\theta \pm 24)$; and d, $\cos^3(\theta)$. The solid curve is the summation of the components.

In the inhibited region, the signal followed a $\cos^{1.3}(\theta)$ form, close to a cosine distribution.

As shown in the next section, the velocity distribution always involves the thermalized component yielding a cosine distribution. Therefore, the angular distribution was deconvoluted into a cosine form and the sharp distribution components consisting of the remaining signal. In active A, referring to the deconvolution of the velocity curve, the signal was approximated as $0.55 \cos^4(\theta) + 0.14 \cos(\theta)$. In active B, it was approximated as $1.40 \cos^{10}(\theta + 24) + 1.40 \cos^{10}(\theta - 24) + 1.0 \cos(\theta)$. For CO pressures close to the kinetic transition, the cosine component was enhanced. The signal in the inhibited region was described as $0.20 \cos^3(\theta) + 0.80 \cos(\theta)$.

C. Velocity Distribution. In the above three regions showing different angular distributions, velocity distributions of desorbing CO_2 and LEED structures were examined.

The velocity distribution curves at different desorption angles are shown in Figure 3a−c. The curve always showed a single peak except for the active B region. In this region, the velocity distribution became broad, yielding a value of about 1.2 at $\theta = 0-24°$ as the speed ratio (SR) which was defined as $((\langle v^2 \rangle / \langle v \rangle^2) - 1)^{1/2} / (32/9\pi - 1)^{1/2}$, where v is the velocity of the molecule, $\langle v \rangle$ is the mean velocity, and $\langle v^2 \rangle$ is the mean square velocity.[25] Furthermore, the average kinetic energy was maximized at a collimation angle of 24°. These strongly suggest the presence of two desorption components with different velocity distributions because the SR value usually becomes

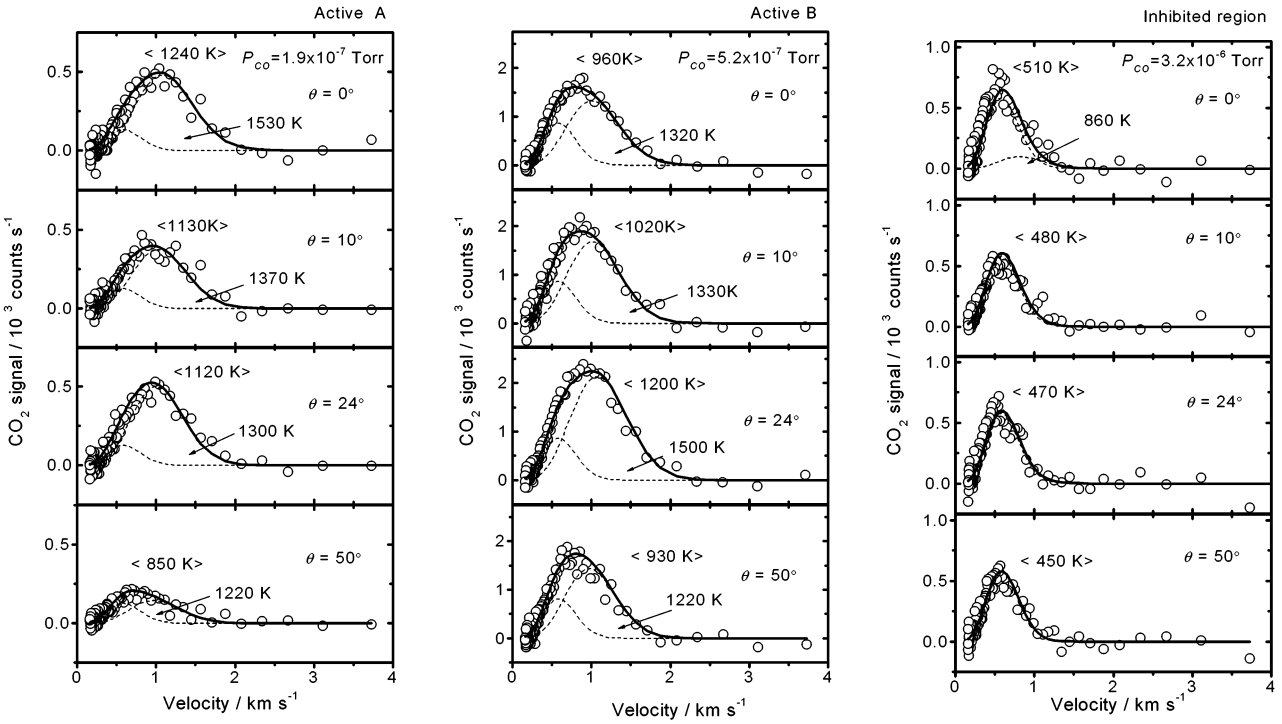

Figure 3. Velocity distributions of desorbing CO_2 at different desorption angles at $T_S = 450$ K and $P_{O_2} = 1.0 \times 10^{-6}$ Torr in active A, active B, and the inhibited region. The temperature in < > shows the mean translational energy in temperature units over all CO_2 molecules. Typical deconvolutions are shown by broken curves. The solid curve is the summation of the components.

less than unity at the collimation position for a single desorption component with excess energy.

Thus, the data were first fit to the Maxwell form at the surface temperature, and the remaining signal after the subtraction of the slow component was fitted to a modified Maxwell form. A typical deconvolution is shown by broken curves in the Figure. The resultant energy is indicated (in temperature units) as $T\langle E\rangle = \langle E\rangle/2k_B$, where $\langle E\rangle$ is the mean translational energy and k_B is the Boltzmann constant. The SR value of the resultant fast component reached 0.95 at $\theta = 24°$ in region B, being reasonable as the hyperthermal component of product CO_2.[26]

In active A, the observed translational temperature without deconvolution was maximized in the normal direction, reaching about 1240 K. It decreased to 850 K at $\theta = 50°$ with increasing desorption angle. The translational temperature of the fast component obtained in the deconvolution was maximized to 1530 K in the normal direction and decreased with increasing desorption angle. However, in active B, the translational temperature of the fast component was maximized at $\theta = 24°$, reaching 1500 K. It decreased with increasing shift from the collimation angle, being consistent with observed bidirectional desorption. In the inhibited region, the velocity distribution was mostly described as a Maxwell form at the surface temperature over the desorption angles studied, consistent with the cosine distribution.

D. LEED Study. Clean Rh(110) showed a sharp (1 × 1) LEED pattern. The well-known (2 × 2)p2mg-O structure (Figure 4a) appeared when the surface was exposed to O_2 at $T_S = 450$ K.[9,10] With increasing CO pressure, the half-order spots due to (1 × 2) (Figure 4b) were superimposed around the boundary between active A and B and disappeared close to the kinetic transition. The intensities of the spots marked in Figure 4 were monitored by a CCD video system at an acceleration voltage of 139 eV. The LEED patterns were taken over a long integration of 3 s because the beam current was reduced to the level of nonvisible spots. Such measurements were performed

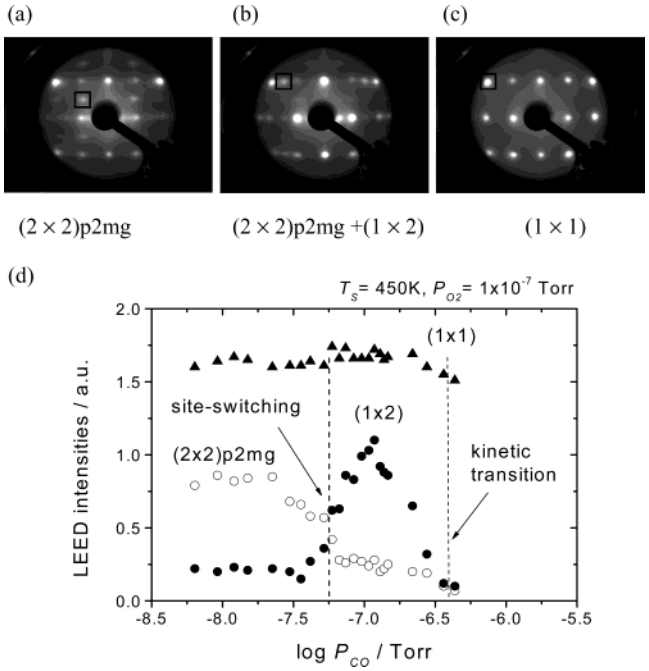

Figure 4. Typical LEED patterns in (a) active A, (b) active B, and (c) the inhibited regions. (d) Spot intensities of (2 × 2)p2 mg, (1 × 2), and one of the integral orders as a function of CO pressure at $T_S = 450$ K and $P_{O2} = 1 \times 10^{-7}$ Torr. The vertical lines indicate the site-switching and kinetic transition points.

after the steady-state reaction condition had been established. The intensity of one of the half-order spots was plotted against CO pressure in Figure 4d. It increased sharply at the boundary between active A and B and was maximized around the middle of active B. It was almost suppressed at the kinetic transition. However, the intensity of (2 × 2)p2mg was fairly constant in active A and sharply suppressed in active B. Above the kinetic transition point, a clear (1 × 1) pattern (Figure 4c) was observed.

No changes were found in the spot intensity due to the integral order.

IV. Discussion

A. Slow Component. The CO_2 desorption on the present surface is divided into two channels (i.e., the product is either desorbed before accommodation or emitted after complete thermalization to the surface temperature).

On the present surface, the bimodal distributions disappear in the inhibiting region (i.e., the angular distribution of desorbing CO_2 approaches a cosine form and the velocity distribution shows a Maxwell distribution at the surface temperature). The product CO_2 molecules are thermalized to the surface temperature before desorption. This is very similar to the results on Pd(110),[27] on which the fast component predominant in the active region was mostly suppressed above the kinetic transition (i.e., only the slow component remained in the inhibited region). On the present surface, even in the active region the slow component is significant. By considering the differences in angular and velocity distributions between the two components,[28] the slow component was estimated in active A to be about 40% of the total formation. In active B, the slow component reached about 80%. The value increased with increasing CO pressure. This large contribution of the slow component obscures the observation of the inclined desorption.

Adsorbed CO moves quickly on the surface at reaction temperatures.[29] CO_2 formation is likely to take place on oxygen adsorption sites.[3] At small coverage, oxygen adatoms might be distributed on or close to oxygen dissociation sites because the site yields a higher binding energy and the surface diffusion of oxygen atoms is slow.[30] This suggests that the CO_2 formation place will shift toward the site for oxygen dissociation when the surface lacks oxygen (i.e., in the inhibited region). The fraction of the slow component increased in the order of active A < active B < inhibited region. This suggests that the slow component is formed on the sites for oxygen dissociation or nearby. O_2 dissociation is likely to occur on sites yielding a higher binding energy of oxygen molecules. Thus, structural defects on the surface may be invoked for the reaction site of the slow component. Such defects may be created on Rh(110) because this surface is reconstructed by oxygen adsorption and returned to the (1×1) form after the removal of oxygen by CO.[16]

B. Bidirectional Desorption. The observed bidirectional desorption is reminiscent of the results on Pt(110)(1×2), where the product CO_2 desorption is clearly split at low CO coverage in TDS work[22] and also under steady-state CO oxidation conditions.[24] On Pt(110), the bidirectional desorption is found in the wide coverage range of oxygen because the surface keeps a well-ordered missing-row structure even if it is covered by oxygen. These resultant declining terraces with a (111) structure provide 3-fold hollow sites suitable for oxygen adsorption.[31] This oxygen seems to be more reactive toward CO than that on Pt(110)(1×1) because CO_2 formation takes place predominantly on (1×2) domains until the domains are mostly suppressed.[24] The collimation angle of 25° is shifted from the local normal direction of the declining terraces by about 5°.[3] This was already explained by the surface-smoothing effect due to conduction electrons.

However, no bidirectional CO_2 desorption was observed on Rh(110) in TDS work.[8] The bidirectional desorption was found only in the limited CO pressure range under steady-state catalyzed conditions. The oxygen coverage during this observation of bidirectional desorption is probably less than half a monolayer because the intensity of the (2×2)p2 mg-O pattern, which involves 0.5 monolayer oxygen,[10] remained constant below the site switching. However, in active B, the (2×2)p2 mg-O lattice was suppressed, and the half-order LEED spot intensity was maximized. This indicates the presence of the metastable (1×2) missing-row structure during steady-state conditions. This metastable structure was proposed to be a (1×2) missing row after the removal of O(a) induced the reconstruction by CO or hydrogen treatment at 370 K.[15,16] It can be converted into the (1×1) form by heating at surface temperatures above 480 K. The appearance of this structure is reasonable because the surface oxygen content is reduced below the critical CO pressure. The metastable (1×2) structure may be chemically active and enhance CO_2 formation, as observed on Pt(110)(1×2).[24]

C. Normally Directed Desorption. In active A, CO_2 desorption collimated along the surface-normal direction. The surface showed the (2×2)p2 mg LEED pattern. On this lattice, oxygen was proposed to occupy the fcc 3-fold sites in a zigzag arrangement along the $[1\bar{1}0]$ troughs.[32] Recent STM work indicates that this zigzag chain extends along the $[1\bar{1}0]$ direction[11] (i.e., oxygen is involved in some assemblies on the surface and is not randomly distributed). A lack of bidirectional desorption and less reactivity in active A may be expected when oxygen on the terminal of the zigzag chain is more reactive to CO and the resultant CO_2 is emitted from the end of the chain. This would reduce the CO_2 productivity because CO adsoption is retarded on the chain and most of the CO(a) is not distributed close to the chain end. Such CO_2 formation is not inconsistent with the normally directed emission because the desorption of bulky CO_2 from the inclined terrace may be affected by the zigzag chain on the nearest terrace.

There are differences in oxygen adsorption between Pt(110) and Rh(110). The (1×2) structure on Pt(110) does not change by oxygen adsorption, and oxygen coverage does not exceed the 0.35 monolayer.[33] O(a) is highly populated on declining terraces over a wide coverage range.[31] This surface still can adsorb significant amounts of CO. This means that the reaction is not retarded by CO in the active region on Pt(110).[24] However, on Rh(110), oxygen is likely to form chainlike assemblies over a wide coverage range and retard CO oxidation even in the active region.

V. Summary

The angular and velocity distributions of desorbing product CO_2 were measured in steady-state CO oxidation on Rh(110), and LEED spot intensities were monitored under the same conditions. In a limited CO pressure range in the active region, CO_2 productivity was enhanced, and CO_2 desorption was split into inclined lobes nearly along the local normal of the declining terraces of the missing-row structure. At the same time, the (1×2) LEED pattern due to the missing-row structure was confirmed, indicating this enhanced CO_2 formation on inclined terraces. The metastable (1×2) missing-row structure was proposed to be responsible for this formation.

Acknowledgment. I.I.R. is indebted to the Ministry of Education, Science, Sports, and Culture of Japan for a 2000−2004 scholarship. This work was supported in part by Grant-in-Aid no. 13640493 for General Scientific Research from the Japan Society of the Promotion of Science.

References and Notes

(1) Becker, Ch. A.; Cowin, J. P.; Wharton, L.; Auerbach, D. J. *J. Chem. Phys.* **1977**, 67, 3394.

(2) Colonell, J. I.; Gibson, K. D.; Sibner, S. J. *J. Chem. Phys.* **1995**, 103, 6677.
(3) Matsushima, T. *Heterog. Chem. Rev.* **1995**, *2*, 51.
(4) Besenbacher, F.; Stensgaard, I. In *Phase Transitions and Adsorbate Reconstructing at Metal Surfaces*; King, D. A., Woodruff, D. P., Eds.; Chemical Physics of Solid Surfaces; Elsevier: Amsterdam, 1994; Vol. 7, p 573.
(5) Matsushima, T. *J. Chem. Phys.* **1990**, *93*, 1464.
(6) Matsushima, T.; Ohno, Y.; Nagai, K. *J. Chem. Phys.* **1991**, *94*, 704.
(7) Matsushima, T. *J. Chem. Phys.* **1989**, *91*, 5722.
(8) Matsushima T.; Ohno, Y. *Catal. Lett.* **1994**, *23*, 313.
(9) Comelli, G.; Dhanak, V. R.; Kiskinova, M.; Paolucci, G.; Prince, K. C.; Rosei, R. *Surf. Sci.* **1992**, *269/270*, 360.
(10) Comelli, G.; Dhanak, V. R.; Kiskinova, M.; Prince, K. C. Rosei, R. *Surf. Sci. Rep.* **1998**, *32*, 165.
(11) Vesselli, E.; Africh, C.; Baraldi, A.; Comelli, G.; Esch, F.; Rosei, R. *J. Chem. Phys.* **2001**, *114*, 4221.
(12) Matsushima, T.; Shobatake, K.; Ohno, Y.; Tabayashi, K. *J. Chem. Phys.* **1992**, *97*, 2783.
(13) Matsushima, T.; Almy, D. B.; White, J. M. *Surf. Sci.* **1977**, *67*, 89.
(14) Ehsasi, M.; Matloch, M.; Frank, O.; Block, J. H.; Christmann, K.; Rys, F. S.; Hirschwald, W. *J. Chem. Phys.* **1989**, *91*, 4949.
(15) Dhanak, V. R.; Comelli, G.; Cautero, G.; Paulucci, G.; Prince, K. C.; Kiskinova, M.; Rosei, R. *Chem. Phys. Lett.* **1992**, *188*, 237.
(16) Comelli, G.; Dhanak, V. R.; Kiskinova, M.; Pangher, N.; Paolucci, G.; Prince, K. C.; Rosei, R. *Surf. Sci.* **1992**, *260*, 7.
(17) Makaeev, A.; Imbihl, R. *J. Chem. Phys.* **2000**, *113*, 3854.
(18) Kobal, I.; Rzeźnicka, I.; Matsushima, T. *Recent Res. Dev. Phys. Chem.* **2002**, *6*, 391.
(19) Cao, G.; Seimiya, Y.; Matsushima, T. *J. Mol. Catal.* **1999**, *141*, 63.
(20) Comsa, G.; David, R.; Schumacher, B. J. *Rev. Sci. Instrum.* **1981**, *52*, 789.
(21) Ohno, Y.; Matsushima, T.; Miki, H. *Surf. Sci.* **1993**, *281*, 234.
(22) Ohno, Y.; Matsushima, T.; Uetsuka, H. *J. Chem. Phys.* **1994**, *101*, 5319.
(23) Brown, L. S.; Sibner, S. J. *J. Chem. Phys.* **1989**, *90*, 2807.
(24) Rzeznicka, I.; Morales de la Garza, L.; Matsushima, T. *J. Vac. Sci. Technol.* **2002**, *20*, 1475.
(25) Comsa, G.; David, R. J. *Surf. Sci. Rep.* **1985**, *5*, 145.
(26) Ohno, Y.; Matsushima, T. *J. Chem. Phys.* **1994**, *101*, 5319.
(27) Moula, Md. G.; Wako, S.; Cao, G.; Kimura, K.; Ohno, Y.; Kobal, I.; Matsushima. T. *Phys. Chem. Chem. Phys.* **1999**, *1*, 3677.
(28) Cao, G.; Moula, M. G.; Ohno, Y.; Matsushima, T. *J. Phys. Chem. B* **1999**, *103*, 3235.
(29) Reutt-Robey, J. E.; Doren, D. J.; Chabal, Y. J.; Christman, S. B. *Phys. Rev. Lett.* **1988**, *61*, 2778.
(30) von Oertzen, A.; Rotermund, H. H.; Nettesheim, S. *Surf. Sci.* **1994**, *311*, 322.
(31) Schmidt, J.; Stuhlmann, Ch.; Ibach, H. *Surf. Sci.* **1993**, *284*, 121.
(32) Muray, P. W.; Leibsle, F. M.; Li, Y.; Guo, Q.; Bowker, M.; Thorton, G.; Dhank, V. R.; Prince, K. C.; Rosei, R. *Phys. Rev. B* **1993**, *47*, 12976.
(33) Freyer, N.; Kiskinova, M.; Pirug, G.; Bonzel, H. P. *Surf. Sci.* **1986**, *166*, 206.